Available online at www.sciencedirect.com
SCIENCE DIRECT®
Infrared Physics & Technology 46 (2005) 418–428
INFRARED PHYSICS & TECHNOLOGY
www.elsevier.com/locate/infrared

Comparison of dipole, bowtie, spiral and log-periodic IR antennas

F.J. González [a,*], G.D. Boreman [b]

[a] Instituto de Invesigación en Comunicación Optica, Universidad Autónoma de San Luis Potosí, Alvaro Obregón 64, San Luis Potosí, S.L.P., México
[b] School of Optics/CREOL, University of Central Florida, 4000 Central Florida Blvd., Orlando, FL 32816-2700, USA

Received 30 August 2004
Available online 10 November 2004

Abstract

Antenna-coupled microbolometers use planar lithographic antennas to couple infrared radiation into a bolometer with sub-micron dimensions. In this paper four different types of infrared antennas were fabricated on thin grounded-substrates and coupled to microbolometers. Dipole, bowtie, spiral and log-periodic IR antenna-coupled detectors were measured at 10.6 μm and their performance compared. A new method to calculate the radiation efficiency based on the spatial and angular response of infrared antennas is presented and used to evaluate their performance. The calculated radiation efficiency for the dipole, bowtie, spiral and log-periodic IR antennas was 20%, 37%, 25% and 46% respectively. A dipole-length study was performed and shows that the quasistatic value of the effective permittivity accurately describes the incident wavelength in the substrate at infrared frequencies for antennas on a thin substrate.

Keywords: Microbolometer; Infrared antennas; Antenna efficiency; Antenna-coupled detectors

1. Introduction

Antenna-coupled microbolometers use planar lithographic antennas to couple incident radiation into a bolometer with sub-micron dimensions. The use of an antenna limits the throughput to one mode with one polarization. This limitation to one mode is potentially useful for bolometers used for diffraction limited observations over a broad spectral range. Planar antennas, which are built on a substrate, are quite different from ordinary microwave antennas mainly because they tend to radiate most of their energy into the substrate.

* Corresponding author. Tel.: +52 444 825 0183x232; fax: +52 444 825 0198.
E-mail address: javier@cactus.iico.uaslp.mx (F.J. González).

1350-4495/$ - see front matter © 2004 Elsevier B.V. All rights reserved.
doi:10.1016/j.infrared.2004.09.002

For a planar antenna the power division in each medium varies approximately as $\varepsilon^{\frac{3}{2}}$ [1].

Surface wave excitation occurs in all substrate-based antennas because the lowest TM_0 surface wave mode has a zero frequency cutoff [2], by increasing the substrate thickness more surface wave modes appear which will reduce the efficiency of the antenna. At infrared frequencies (THz) the substrates are electrically thicker making antennas less efficient than their lower frequency counterparts. Antennas on grounded substrates are more efficient than printed antennas because they radiate in only one direction and the substrate thickness can be reduced to increase efficiency, this does not happen with printed antennas which can be viewed as microstrip antennas with very thick substrates. The radiation properties of printed antennas become sensitive to substrate losses as the substrate thickness increases [3].

The performance of printed antennas depends on the substrate thickness (h) and the dielectric constant of the substrate (ε_s) [4], and there is a certain thickness that will maximize the performance of a printed antenna for a given dielectric constant. For a half-wave dipole the maximum efficiency is obtained when $h \approx 0.2\lambda_0$ (where λ_0 is the free-space wavelength) which is slightly below the cut-off thickness of the TE_0 substrate guided mode [2], and the efficiency is close to 100% when the substrate thickness is close to zero because surface wave excitation is negligible for very thin substrates.

In this paper four different types of infrared antennas were fabricated on thin grounded-substrates and coupled to microbolometers. Dipole, bowtie, spiral and log-periodic IR antenna-coupled detectors were measured at 10.6 μm and their performance compared.

2. Method

Fabrication was done on 200 nm of SiO_2 ($\varepsilon_s = 4.84$ at 10.6 μm) deposited using PECVD over a 50 nm Cr ground plane. The substrate thickness is much smaller than the wavelength in the dielectric ($h \approx 0.04\lambda_d$, where $\lambda_d = \frac{\lambda_0}{\sqrt{\varepsilon_s}}$). Antennas were made out of 100 nm-thick gold and patterned using electron beam lithography and liftoff, and 70 nm of dc-sputtered niobium was used as the bolometric element.

Testing of the devices was done using a CO_2-laser at 10.6 μm. focused by an F/8 optical train which had an almost diffraction-limited spot with a $1/e^2$ radius of 200 μm a power at the focal plane of 43.4 mW and an irradiance of 117 W/cm^2. The polarization was linear and was rotated using a half-wave plate, all the measurements were made at the optimum polarization where the maximum response was obtained. Noise, response, angular and time constant measurements were made using the same procedure explained in [5].

To obtain the spatial response of lithographic infrared antennas the deconvolution method developed by Alda et al. [6] was used. This method deconvolves a theoretical model of the laser beam with two-dimensional scans in the infrared of the antennas. The laser beam is modeled as a 2D Gaussian beam convolved with a slightly comatic Airy function. The analytical beam model is obtained by fitting the characteristics of the real laser beam obtained by knife-edge measurements.

3. Results

3.1. Dipoles

A half-wavelength dipole can be made to resonate and show a purely real input impedance, thus eliminating the need for tuning to achieve a conjugate impedance match. The resonant condition for a half-wave dipole is that the physical length must be shorter but close to half the wavelength and as the antenna cross-arm thickness is increased the length must be reduced more to achieve resonance.

Infrared dipole antennas coupled to Nb microbolometers were fabricated on a 200 nm SiO_2 grounded substrate using electron-beam lithography and liftoff (Fig. 1). The grounded substrate is thin enough to reduce losses due to surface waves.

Fig. 2 shows the response of dipole-coupled microbolometers as a function of dipole length, we can see how the maximum response is around 3 μm which is close to half the effective wavelength.

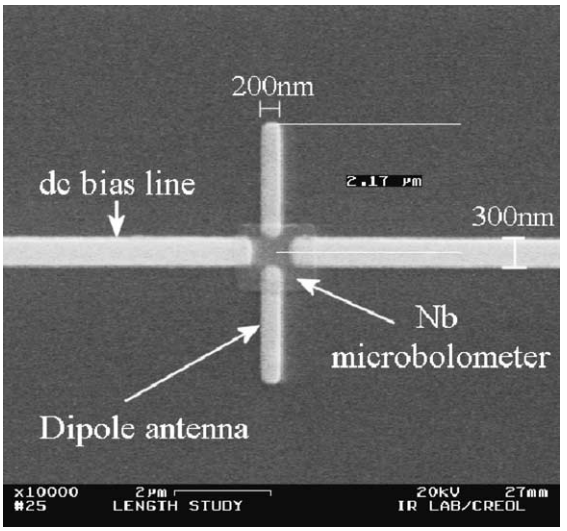

Fig. 1. Dipole-coupled microbolometer.

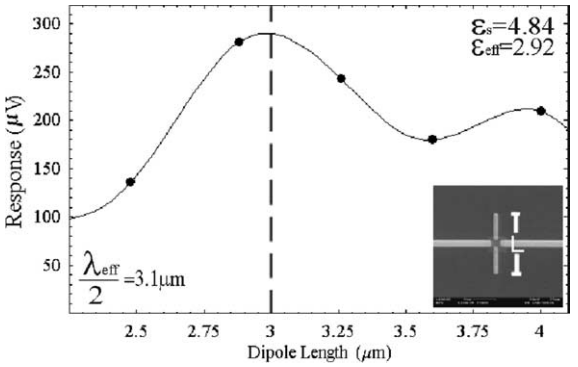

Fig. 2. Response of a microstrip dipole as a function of its length.

For a 200 nm SiO_2 substrate at 10.6 μm the effective permittivity is equal to its quasi-static value ($\varepsilon_{\text{eff}} = \frac{\varepsilon_s+1}{2}$) [7], since the permittivity of SiO_2 is $\varepsilon_s = 4.84$ at 10.6 μm then the effective permittivity is given by $\varepsilon_{\text{eff}} = 2.92$ which gives an effective wavelength in the substrate equal to $\lambda_{\text{eff}} = \frac{\lambda_0}{\sqrt{\lambda_{\text{eff}}}} = \frac{10.6\ \mu\text{m}}{1.7} = 6.2\,\mu\text{m}$ according to this, the first resonance of the dipole should be around $\frac{\lambda_{\text{eff}}}{2} = 3.1\,\mu\text{m}$ which agrees with the results shown in Fig. 2.

The polarization dependence of dipole-coupled microbolometers was measured using a half-wave plate and is shown in Fig. 3, the maximum response was obtained when the polarization was parallel to the antenna axis. The response as a function of polarization angle presented a cosine squared dependence which agrees with antenna theory, the ratio of maximum to the minimum polarization response (polarization ratio) of these devices was around 4.

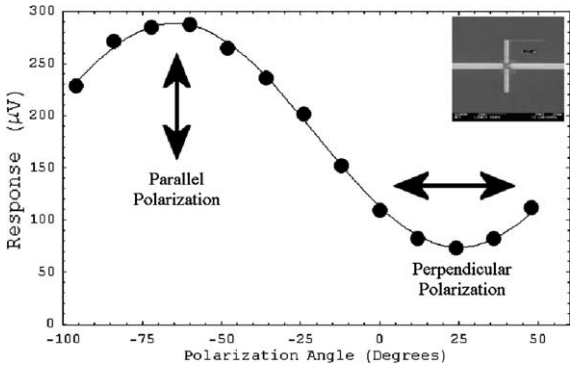

Fig. 3. Polarization dependence for a dipole-coupled microbolometer.

A two-dimensional scan over the dipole-coupled microbolometer was performed using an *F*/1 beam at 10.6 μm and is shown in Fig. 4(a), this figure represents a convolution between the detector's spatial response and the laser beam profile. The collection area of the detector is obtained by deconvolving the two-dimensional scan with the laser beam profile (Fig. 4(b)).

Fig. 4(b) represents the spatial response of the detector to 10.6 μm radiation, if we approximate the spatial response to a 3D-Gaussian function we can determine that 85% of the total volume of the Gaussian is enclosed under the 0.2 *z*-contour level. If we define the collection area as the area where 85% of the collected energy falls, then from Fig. 4(b) we can determine that the collection area of these dipole-coupled microbolometers is approximately 10 μm^2.

Fig. 5 shows the radiation pattern of a dipole-coupled niobium microbolometer. The effective collection area is related to the maximum directivity of an antenna by the following equation [8]:

$$A_{\text{eff}} = \frac{\lambda^2 D_{\max}}{4\pi}, \tag{1}$$

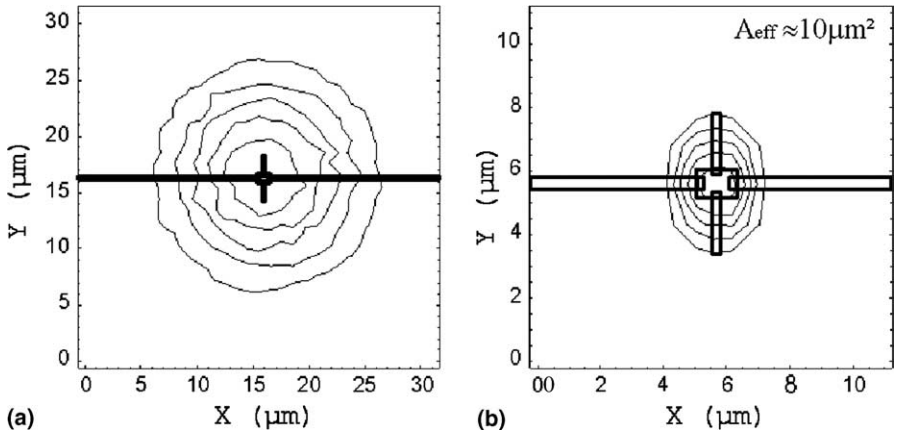

Fig. 4. Dipole spatial response (a) convolved with the laser beam, (b) after deconvolution. The contours represent 15% increments.

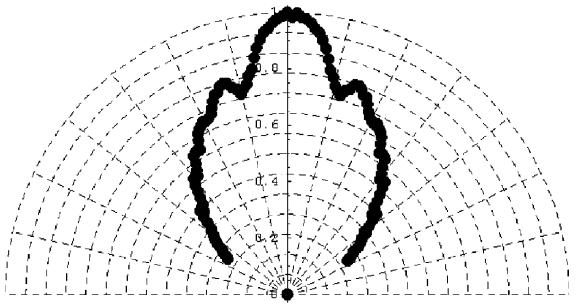

Fig. 5. Radiation pattern of a dipole-coupled microbolometer.

where the maximum directivity of the antenna is defined as the ratio of the maximum radiation intensity to the radiation intensity averaged over all directions. And the maximum directivity is related to the power pattern through the following equation [8]:

$$D_{\max} = \frac{4\pi U_{\max}}{P_{\text{rad}}}, \tag{2}$$

where $U_{\max}$ is the maximum radiation intensity and P_{rad} is the total radiated power. If we want to calculate the directivity of a printed antenna in the normal direction, then $U_{\max}$ will be the value of the power pattern at 90° and the total power can be obtained by calculating the volume under the power pattern $P(\theta)$,

$$P_{\text{rad}} = 2\pi \int_0^{\pi} P(\theta)\sin(\theta)\,\mathrm{d}\theta. \tag{3}$$

Eq. (3) assumes that the power pattern is omnidirectional (it does not depend on the spherical coordinate ϕ). For a more accurate calculation of the total power radiated by an antenna a three-dimensional radiation pattern (θ, ϕ) needs to be measured.

By using Eqs. (1)–(3) on the power pattern shown in Fig. 5 we find that the directivity in the normal direction for this dipole antenna is 1.7 and the calculated effective area is around $52\,\mu\text{m}^2$, the difference between measured and calculated effective areas is due to reflection and dielectric conduction losses, therefore the radiation efficiency of this antenna is the ratio of measured and calculated effective areas, which is around 20%.

These dipole-coupled niobium microbolometers presented an average dc-resistance of $80 \pm 5\,\Omega$, the measured response to the incident infrared radiation was around $11 \pm 2\,\mu\text{V}$ for the polarization parallel to the dipole antenna, the noise was around 29 $\frac{\text{nV}}{\sqrt{\text{Hz}}}$, which gives a signal-to-noise ratio (SNR) of ~380, a responsivity of 0.8 V/W and a D^* of 8.6×10^3 $\frac{\text{cm}\sqrt{\text{Hz}}}{\text{W}}$.

3.2. Bowties

If an antenna is made using perfect conductors and dielectrics and its dimensions change, the characteristics of that antenna (impedance, polarization, radiation pattern, etc) will remain the same

as long as the wavelength of operation is changed in the same amount. Therefore, if the shape of an antenna is determined only by angles, the performance of that antenna would be independent of frequency since it would be invariant to a change of scale [9], bowties, spirals and log-periodic antennas are examples of frequency independent antennas.

The main advantages of bowtie antennas are simple design and broad-band impedance. A bowtie antenna is made from a bitriangular sheet of metal with the feed at its vertex. This type of antenna, which is only defined by the bow angle θ, would be frequency independent if it extended to infinity on both sides. To fabricate a practical bow-tie antenna we must have a finite gap between the feed points and a finite size which would result in limited bandwidth, however typically the antenna can be terminated with a bow-arm length of $2\lambda_{\text{eff}}$ without a significant effect on the pattern or the impedance [10].

The radiation of a bowtie antenna is linearly polarized and has a bidirectional pattern with broad main beams perpendicular to the plane of the antenna. The impedance can be calculated accurately from transmission line theory [11] and is given by

$$Z = \sqrt{\frac{2\mu_0}{\varepsilon_{\text{eff}} + \varepsilon_0}} \cdot \frac{K(k)}{K'(k)}, \tag{4}$$

where

$$K(k) = \int_0^1 \frac{\mathrm{d}x}{\sqrt{(1-x^2)(1-k^2x^2)}},$$

$$K'(k) = K(k') \tag{5}$$

and

$$k' = \sqrt{1-k^2}. \tag{6}$$

K and K' are elliptic integrals of the first kind, $k = \tan^2(45° - \theta/4)$ and θ is the bow angle. Fig. 6 shows the impedance of a bowtie antenna on a silicon substrate as a function of the flare angle, this impedance is purely real for any bow angle, this behavior has been demonstrated experimentally in [11].

Fig. 7 shows an electron micrograph of a planar bowtie antenna similar to the one used in this study. The antenna is 4 μm long and has a bow angle of around 60° which would yield an impedance close to 75 Ω, intended to match the impedance of the sensing Nb patch.

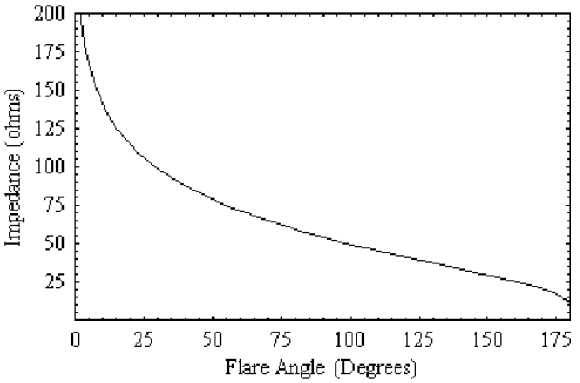

Fig. 6. Impedance of a bowtie antenna on a silicon substrate as a function of the flare angle.

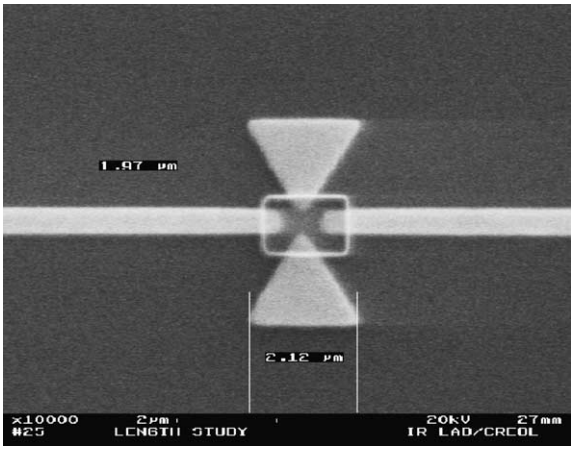

Fig. 7. Bowtie-coupled microbolometer.

Fig. 8 shows the polarization response of a bowtie-coupled microbolometer, this response also follows a cosine squared dependence, characteristic of linearly polarized antennas and it presented a polarization ratio close to 17.

Fig. 9(a) and (b) show a two-dimensional scan over a bowtie-coupled microbolometer and the spatial response of the same device to 10.6 μm radiation after deconvolution. From Fig. 9(b) we can see that the effective collection area of the bowtie-coupled microbolometer is close to $\sim 14\,\mu\text{m}^2$.

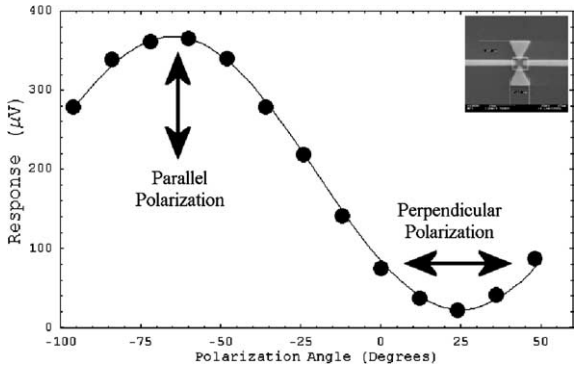

Fig. 8. Polarization dependence for a bowtie-coupled microbolometer.

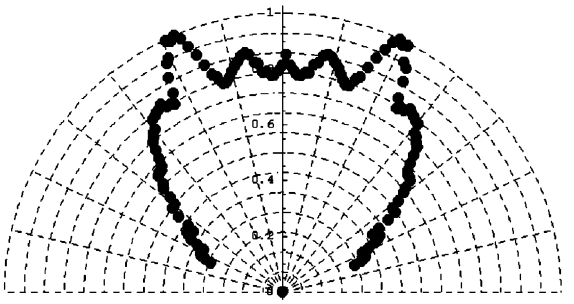

Fig. 10. Radiation pattern of a bowtie-coupled niobium microbolometer.

Fig. 10 shows the radiation pattern of a bowtie-coupled niobium microbolometer, the directivity in the normal direction for this power pattern is 1.2 and the calculated effective area is around $37.5\,\mu m^2$ the radiation efficiency of this antenna, comparing the calculated and the measured effective area, is around 37%.

These bowtie-coupled niobium microbolometers presented an average dc-resistance of $90 \pm 5\,\Omega$, the measured response to the incident infrared radiation was around $14 \pm 1\,\mu V$ for the polarization parallel to the bowtie antenna, the noise was around 29 $\frac{nV}{\sqrt{Hz}}$, which gives a signal-to-noise ratio (SNR) of ~482, a responsivity of 0.72 V/W and a D^* of 9.3 ± 10^3 $\frac{cm\sqrt{Hz}}{W}$.

3.3. Square spirals

The equiangular spiral is a geometrical configuration that can be described just by angles, therefore it fulfills the requirement for shapes that can be used to design frequency independent antennas. The lower limit of their frequency bandwidth depends on the outer circumference of the spiral and the upper frequency limit depends on the configuration near the feed point. Spiral antennas are circularly polarized with a sense that depends on the winding sense of the spirals. A square spiral antenna is regarded as a counterpart of a round spiral antenna with the advantage that it offers a size reduction of 22% (based on the increase of perimeter from πD to 4D) [12]. The radiating characteristics of this antenna can be explained by

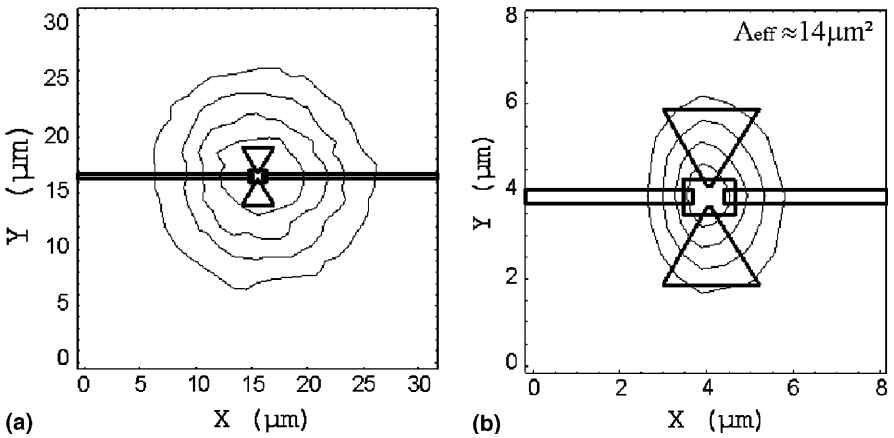

Fig. 9. Bowtie spatial response (a) convolved with the laser beam, (b) after deconvolution. The contours represent 15% increments.

modelling it as a two-wire transmission line. A current wave traveling along the arms of the antenna radiates energy which decreases the amplitude of the current along the conducting antenna arms, and beyond a certain point the presence or absence of the conductor makes little difference. The point of negligible current occurs about one wavelength from the feed point [13], therefore when the wavelength is shorter than the arm length, the performance is practically frequency independent. If the antenna arms become shorter than the wavelength the polarization becomes elliptical where its axial ratio increases by decreasing the arm length until the polarization becomes linear and the spiral becomes a dipole.

Fig. 11 shows the geometry of a two-wire square spiral antenna, the antenna arms A and B are composed of linear filaments wound in the X–Y plane where the length of the nth filament is given by

$$L_n = \begin{cases} a & \text{for } n = 1, \\ 2a(n-1) & \text{for } n = 2, 3, \ldots \end{cases} \tag{7}$$

A planar spiral antenna with arms 17 μm long, 200 nm wide and 100 nm thick made out of gold with a Nb microbolometer in the feed point is shown in Fig. 12. This antenna was fabricated on a 200 nm SiO_2 substrate and a Cr ground plane.

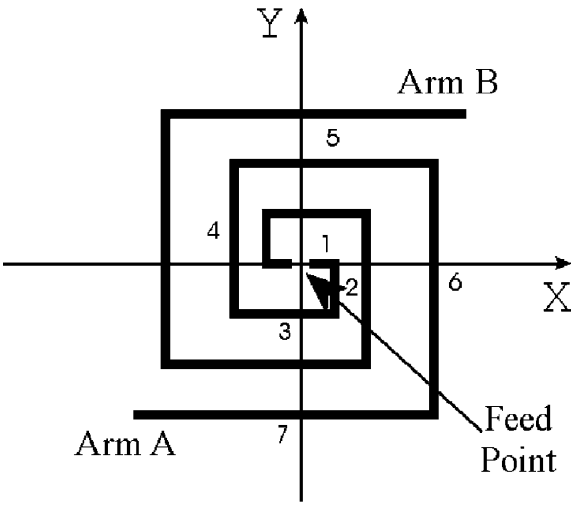

Fig. 11. Geometry of a two-wire square spiral antenna.

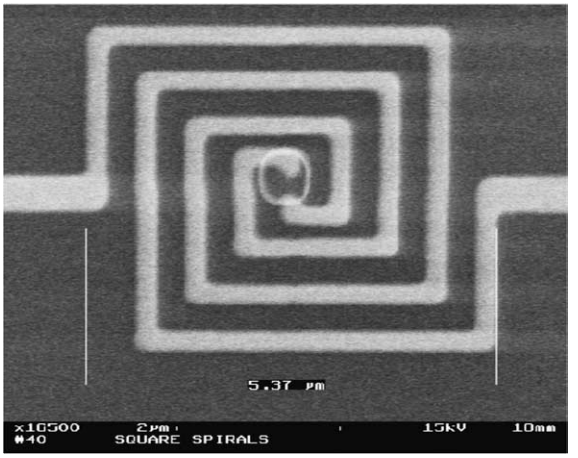

Fig. 12. Spiral-coupled microbolometer.

Fig. 13 shows the polarization response of a square-spiral-coupled microbolometer to linearly polarized radiation at 10.6 μm, spiral antennas have circular polarization for wavelengths smaller than the arm length, this spiral-antenna presented a linear-polarization ratio close to 1.5 which indicates that the polarization of the antenna is actually elliptical, this ellipticity might be due to contributions to the total response of the bias leads acting as long dipoles which are linearly polarized. The orientation of the principal axis of the elliptical polarization corresponds to the angle where the maximum response is found.

Fig. 14(a) and (b) show the two-dimensional scan of a spiral-coupled microbolometer and its

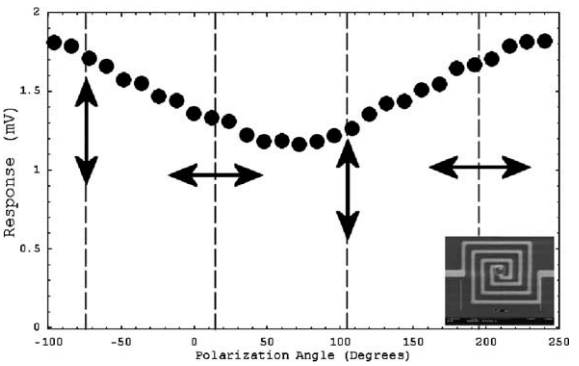

Fig. 13. Polarization dependence of a square-spiral-coupled microbolometer.

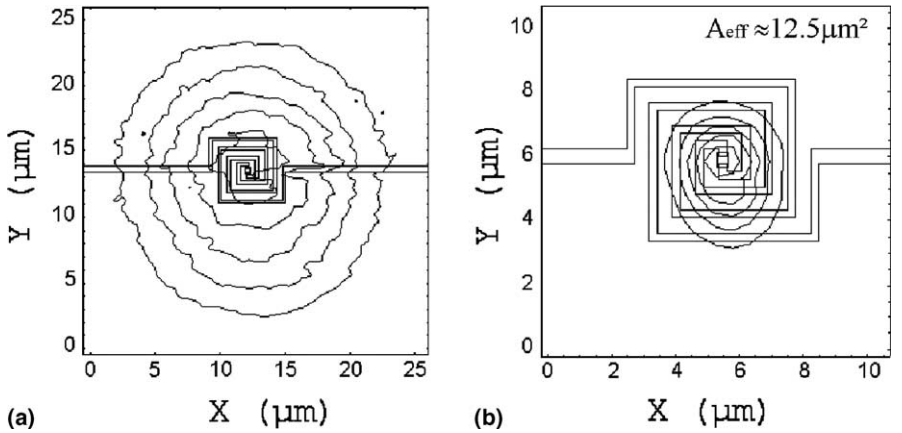

Fig. 14. Spiral spatial response (a) convolved with the laser beam, (b) after deconvolution. The contours represent 15% increments.

deconvolution with the laser beam to find the effective collection area of the detector. From Fig. 14(b) we can see that ~85% of the maximum infrared radiation is collected on an area of $\sim 12.5\,\mu m^2$. Fig. 15 shows the radiation pattern of a spiral-coupled niobium microbolometer, the directivity in the normal direction for this power pattern is 1.6 and the calculated effective area is around $49\,\mu m^2$ which gives a radiation efficiency close to, 25%.

The spiral-coupled niobium microbolometers were measured using a 10.6 μm CO_2 laser and *F*/1 optics, the power at the focal plane was 8.7 mW with an irradiance of $1506\,W/cm^2$, the detectors presented an average de-resistance of $1.4 \pm 0.2\,k\Omega$. The measured response to the incident infrared radiation was around 1.8 ± 0.2 mV, the noise measured was 160 $\frac{nV}{\sqrt{Hz}}$, which gives a signal-to-noise ratio (SNR) of ~11, 250, a responsivity of 9.5 V/W and a D^* of 2.1×10^4 $\frac{cm\sqrt{Hz}}{W}$.

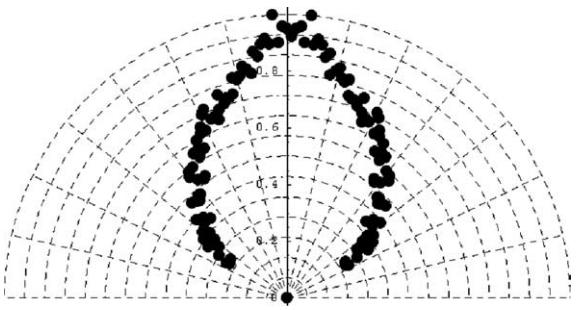

Fig. 15. Radiation pattern of a spiral-coupled niobium microbolometer.

3.4. Log-periodic

If a special kind of repetitiveness in the physical structure of an antenna is introduced a repetitive behavior of the electrical characteristics will be obtained. In log-periodic antennas the geometry is chosen so that the electrical properties repeat themselves with the logarithm of the wavelength. Frequency independence can be obtained when variation of the electrical characteristics over one period is small.

The log-periodic toothed planar antenna is similar to the bowtie antenna except for the teeth. The teeth act to disturb the currents which would flow if the antenna were of bowtie-type construction. The radiation is linearly polarized parallel to the teeth edges, this is perpendicular to what it would be if there were no teeth, in which case the antenna would be a bowtie. This shows that the component of current that flows in the direction of the teeth dominates the radial component [9].

Fig. 16 shows a log-periodic toothed planar antenna, if $\beta_1 + \beta_2 = 90°$ the antenna becomes self-complementary in which case it will have a constant impedance of 189 Ω at all frequencies [9]. Also for a log-periodic toothed planar antenna the ratio of edge distances is constant and is given by the following scale factor:

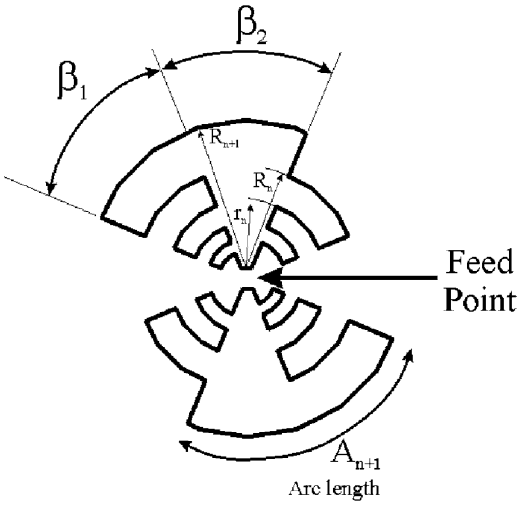

Fig. 16. Log-periodic toothed planar antenna.

$$\tau = \frac{R_{n+1}}{R_n}, \tag{8}$$

the parameter τ gives the period of the structure, therefore a periodic pattern and impedance behavior with the same period would be expected.

Fig. 17 shows an electron micrograph of a planar log-periodic antenna with a scale factor of $\tau \approx 2$ coupled to a niobium microbolometer, this antennas were fabricated on 200 nm of SiO_2 and a chrome ground plane, the antenna and bias lines are made out of 100 nm of evaporated gold and the microbolometer is made out of a 70 nm film of sputtered niobium, the microbolometer is placed at the feed point of the antenna. The antenna is resonant when the length of any of the arcs A_n (as shown in Fig. 16) is equal to $\frac{\lambda_{\text{eff}}}{2}$, the arc length can be calculated as:

$$A_n = \left(\frac{\pi}{2}\right)\left(\frac{R_n + r_n}{2}\right) \tag{9}$$

for $\beta_1 + \beta_2 = 90°$. The corresponding resonant frequencies are:

$$f_n = \frac{2c}{\pi(R_n + r_n)\sqrt{\varepsilon_{\text{eff}}}}. \tag{10}$$

The log-periodic antenna shown in Fig. 17 was designed to have a frequency coverage of 18–70 THz which corresponds to a wavelength coverage of 4–16 μm.

Fig. 18 shows the polarization response of a log-periodic-coupled microbolometer, this response also follows a cosine squared dependence characteristic of linearly polarized antennas, the maximum response is obtained for a polarization parallel to the dc leads which is perpendicular to the polarization of a bowtie and a dipole, the polarization ratio close to 1.4. This low polarization ratio is due to the cross-polarized response given by the bowtie-like part of the log-periodic structure which competes with its co-polarized response, this vector addition of polarizations does not affect the magnitude of the co-polarized response.

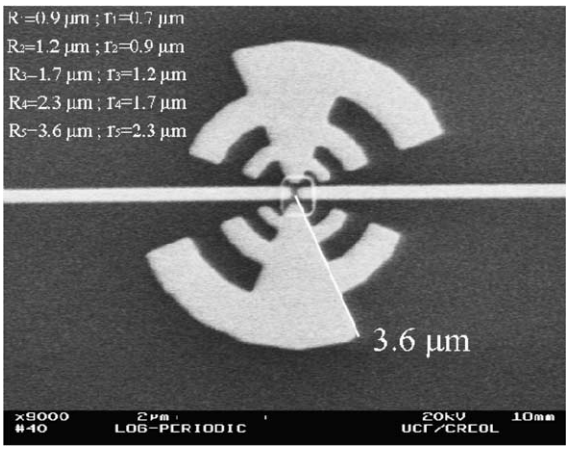

Fig. 17. Log-periodic antenna coupled to a microbolometer.

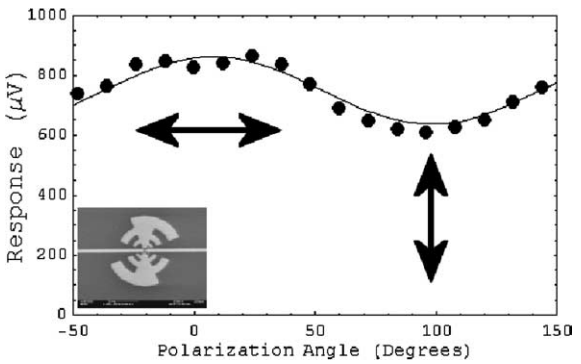

Fig. 18. Polarization dependence for a log-periodic antenna-coupled detector.

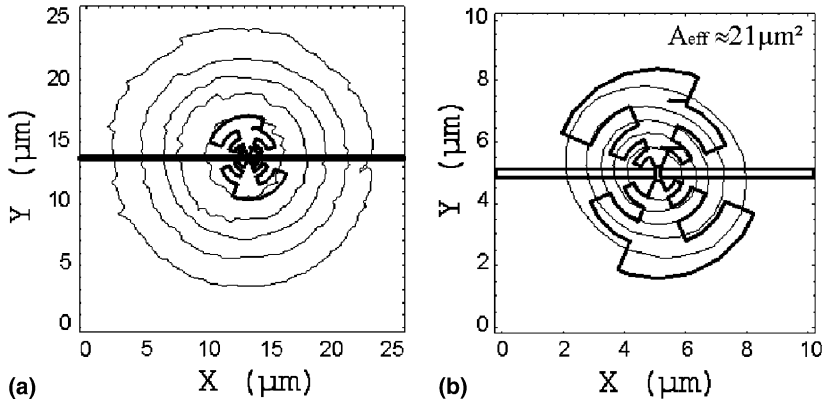

Fig. 19. Spatial response for a log-periodic antenna (a) convolved with the laser beam, (b) after deconvolution. The contours represent 15% increments.

Fig. 19(a) and (b) show the two-dimensional scan of a log-periodic-coupled microbolometer and its deconvolution with the laser beam to find the effective collection area of the detector. From Fig. 19(b) we can see that ~85% of the maximum infrared radiation is collected on an area of $\sim 21\,\mu m^2$. Fig. 20 shows the radiation pattern of a log-periodic-coupled niobium microbolometer, the directivity in the normal direction for this power pattern is 1.5 and the calculated effective area is around $45.6\,\mu m^2$ which gives a radiation efficiency close to 46%.

The log-periodic-coupled niobium microbolometers were measured using a 10.6 μm. CO_2 laser and *F*/1 optics, the power at the focal plane was 8.7 mW with an irradiance of $1506\,W/cm^2$, the detectors presented an average de-resistance of $400 \pm 50\,\Omega$. The measured response to the incident infrared radiation was around 0.9 ± 0.2 mV, the noise measured was 80 $\frac{nV}{\sqrt{Hz}}$, which gives a signal-to-noise ratio (SNR) of ~11250, a responsivity of 2.84 V/W and a D^* of 1.6×10^4 cm $\frac{\sqrt{Hz}}{W}$.

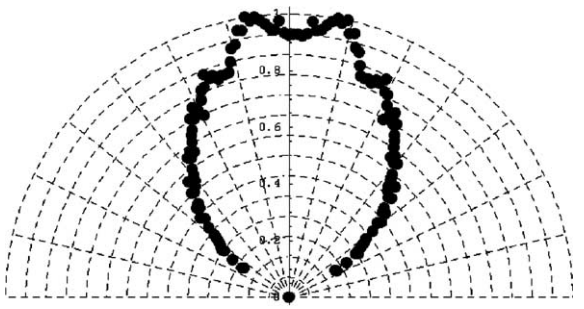

Fig. 20. Radiation pattern of a log-periodic-coupled niobium microbolometer.

4. Conclusions

Four different types of infrared antennas were fabricated on thin grounded-substrates and coupled to microbolometers. Dipole, bowtie, spiral and log-periodic IR antenna-coupled detectors were measured at 10.6 μm and their performance compared.

A dipole-length study showed that the quasi-static value of the effective permittivity accurately describes the incident wavelength in the substrate at infrared frequencies for antennas on a thin substrate.

Values of D^* for the four different types of antennas were similar in magnitude and around 1×10^4 $\frac{cm\sqrt{Hz}}{W}$ for antennas on a substrate, higher D^* values can be achieved by thermally isolating the devices. Polarization response was different for the four antenna geometries, the highest polarization ratios was 17 for the bowtie antenna and 4 for the dipole antenna. A linear-polarization ratio close to 1.5 was obtained for the spiral antenna which indicates that the polarization of the antenna is elliptical and not circular as expected, this ellipticity might be due to contributions to the

total response of the bias leads acting as long dipoles which are linearly polarized. The log-periodic antennas showed a polarization ratio close to 1.4, this low polarization ratio is due to the cross-polarized response given by the bowtie-like part of the log-periodic structure which competes with its co-polarized response.

A new method to calculate the radiation efficiency based on the spatial and angular response of infrared antennas is presented and used to evaluate their performance. The calculated radiation efficiency for the dipole, bowtie, spiral and log-periodic IR antennas was 20%, 37%, 25% and 46% respectively.

Acknowledgments

This work was performed in part at the Cornell Nanofabrication Facility (a member of the National Nanofabrication Users Network) which is supported by the National Science Foundation under Grant ECS-9731293, its users, Cornell University and Industrial Affiliates.

References

[1] C.R. Brewitt-Taylor, D.J. Gunton, H.D. Rees, Planar antennas on a dielectric surface, Electronics Letters 17 (20) (1981) 729–731.

[2] P. Bhartia, K.V.S. Rao, R.S. Tomar, Millimeter-Wave Microstrip and Printed Circuit Antennas, Artech House, 1991.

[3] D.R. Jackson, N.G. Alexopoulos, Microstrip dipoles on electrically thick sub-strates, International Journal of Infrared and Millimeter Waves 7 (1) (1986) 1–26.

[4] P.B. Katehi, N.G. Alexopoulos, On the effect of substrate thickness and permittivity on printed circuit dipole properties, IEEE Transactions on Antennas and Propagation AP-31 (1) (1983) 34–39.

[5] F.J. Gonzalez, M.A. Gritz, C. Fumeaux, G.D. Boreman, Two dimensional array of antenna-coupled microbolometers, International Journal of Infrared and Millimeter Waves 23 (5) (2002) 785–797.

[6] J. Alda, C. Fumeaux, I. Codreanu, J.A. Schaefer, G.D. Boreman, Deconvolution method for two-dimensional spatial-response mapping of lithographic infrared antennas, Applied Optics 38 (19) (1999) 3993–4000.

[7] G. Hasnain, A. Dienes, J.R. Whinnery, Dispersion of picosecond pulses in coplanar transmission lines, IEEE Transactions on Microwave Theory and Techniques 34 (6) (1986) 738–741.

[8] C.A. Balanis, Antenna Theory, John Wiley & Sons, New York, 1997.

[9] V.H. Rumsey, Frequency Independent Antennas, Academic Press, New York, 1966.

[10] D.B. Rutledge, D.P. Neikirk, D.P. Kasilingam, Integrated circuit antennas, Infrared and Millimeter WavesMillimeter Components and Techniques, Part II, vol. 10, Academic Press, New York, 1983, pp. 1–90, Chapter 1.

[11] D.B. Rutledge, M.S. Muha, Imaging antenna arrays, IEEE Transactions on Antennas and Propagation AP-30 (4) (1982) 535–540.

[12] W.L. Stutzman, G.A. Thiele, Antenna Theory and Design, John Wiley & Sons, New York, 1998.

[13] P.E. Mayes, Frequency independent antennas and broadband derivatives thereof, Proceedings of IEEE 80 (1) (1992) 103–112.